NUSC Technical Report 4249

Effectiveness of Damping Tiles for Reducing Vibration of Plates in Water

RUSSEL A. CHRISTMAN
Submarine Sonar Department

WAYNE A. STRAWDERMAN
Office of the Director of Science and Technology

30 May 1972

NAVAL UNDERWATER SYSTEMS CENTER

ADMINISTRATIVE INFORMATION

This study was performed under NUSC Project No. A-702-07 (formerly A-052-00-00), "Flow-Induced Noise Predictions for an Idealized Sonar Dome," Principal Investigator, Dr. W. A. Strawderman, Code TC, and Navy Subproject No. ZR 000 01 01. The sponsoring activity is Chief of Naval Material, Program Manager, Dr. J. H. Huth, DLP/MAT 03L4.

The Technical Reviewer for this report was H. N. Phelps, Code SA22.

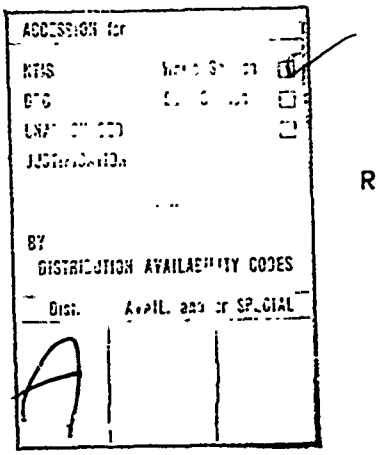

REVIEWED AND APPROVED: 30 May 1972

W. A. Von Winkle
Director of Science and Technology

Inquiries concerning this report may be addressed to the authors,
New London Laboratory, Naval Underwater Systems Center,
New London, Connecticut 06320

UNCLASSIFIED
Security Classification

DOCUMENT CONTROL DATA - R & D

Security classification of title, body of abstract and indexing annotation must be entered when the overall report is classified)

1 ORIGINATING ACTIVITY (Corporate author) Naval Underwater Systems Center Newport, Rhode Island 02840	2a. REPORT SECURITY CLASSIFICATION UNCLASSIFIED 2b GROUP

3 REPORT TITLE

EFFECTIVENESS OF DAMPING TILES FOR REDUCING VIBRATION OF PLATES IN WATER

4 DESCRIPTIVE NOTES (Type of report and inclusive dates)

Research Report

5 AUTHOR(S) (First name, middle initial, last name)

Russell A. Christman
Dr. Wayne A. Strawderman

6 REPORT DATE	7a. TOTAL NO OF PAGES	7b. NO OF REFS
30 May 1972	46	7

8a CONTRACT OR GRANT NO	9a. ORIGINATOR'S REPORT NUMBER(S)
b. PROJECT NO A-702-07 (formerly A-052-00-00) ZR 000 01 01	TR 4249
c d.	9b. OTHER REPORT NO(S) (Any other numbers that may be assigned this report)

10 DISTRIBUTION STATEMENT

Approved for public release; distribution unlimited.

11 SUPPLEMENTARY NOTES	12 SPONSORING MILITARY ACTIVITY
	Department of the Navy

13 ABSTRACT

The effectivenes of damping tiles in reducing the vibration response of a point-excited, clamped-edge plate immersed in water was investigated in a combined theoretical and experimental program. Comparisons of measured acceleration spectra for damped and undamped plates in both air and water environments indicate that damping tiles are less effective in a water environment than in air. A theoretical solution, based on thin-plate theory, of the acceleration power spectral density of a simply supported, fluid-loaded plate is derived and utilized to interpret the experimental results. From the theoretical solution, an approximate theory for plate acceleration in the vicinity of resonance is developed to quantitatively evaluate the effectiveness of damping tiles in a water environment. The combination of theory and experiment reveals that, in a water environment, the forces applied to the plate by the water dominate over those applied by the damping tile, thereby rendering the damping tile less effective in reducing plate vibrations.

DD FORM 1 NOV 65 1473 (PAGE 1)

S/N 0102-014-6600

UNCLASSIFIED
Security Classification

14 KEY WORDS	LINK A		LINK B		LINK C	
	ROLE	WT	ROLE	WT	ROLE	WT
Damping Tests						
Effectiveness						
Plate Vibrations						
Water Loading						

ABSTRACT

The effectiveness of damping tiles in reducing the vibration response of a point-excited, clamped-edge plate immersed in water was investigated in a combined theoretical and experimental program. Comparisons of measured acceleration spectra for damped and undamped plates in both air and water environments indicate that damping tiles are less effective in a water environment than in air. A theoretical solution, based on thin-plate theory, of the acceleration power spectral density of a simply supported, fluid-loaded plate is derived and utilized to interpret the experimental results. From the theoretical solution, an approximate theory for plate acceleration in the vicinity of resonance is developed to quantitatively evaluate the effectiveness of damping tiles in a water environment. The combination of theory and experiment reveals that, in a water environment, the forces applied to the plate by the water dominate over those applied by the damping tile, thereby rendering the damping tile less effective in reducing plate vibrations.

REVERSE BLANK

TABLE OF CONTENTS

LIST OF ILLUSTRATIONS

REVERSE BLANK

LIST OF TABLES

REVERSE BLANK

EFFECTIVENESS OF DAMPING TILES FOR REDUCING VIBRATION OF PLATES IN WATER

INTRODUCTION

The vibration of a ship's hull plating excites a pressure field in the surrounding water. This field is partly responsible for the self- and radiated-noise of the ship, therefore any attempt to reduce the noise should include suppression of hull vibration. This has usually been accomplished by applying damping treatments to the inner surface of the plating in order to dissipate vibrational energy and thereby suppress hull vibration and the consequent radiation of noise.

Inasmuch as pressure levels induced in the surrounding fluid are directly related to hull vibration levels, measurements of reductions in hull vibration levels can provide an indication of the damping tiles' effectiveness.

In the past, laboratory measurements of the effectiveness of damping treatments have been made in air. These measurements do not accurately predict the effectiveness of the same damping treatment applied to a ship's hull because they do not include the effects of the forces induced on the hull by the water environment as a result of the vibration of the hull. These fluid forces may be interpreted[1-3] as additional mass or damping of the plate. Previous investigations[4] of damping effectiveness have attempted to account for the fluid-loading effects by utilizing a theoretically derived correction to the experimental data obtained in air. However, this correction has apparently considered only a portion of the actual fluid-loading forces. This incomplete description may, depending on the material properties of a plating/damping system, lead to error when attempting to extrapolate the effectiveness of damping tiles in water from their effectiveness as measured in air.

The objective of this study was to resolve directly the relationship of fluid forces to the assessment of damping-tile effectiveness; this was accomplished in a two-stage program. First, the vibration responses of damped and undamped finite plates in air and water environments were measured experimentally. Comparison of the responses provided a means for determining the effectiveness of the damping tile, and the experimental data in both environments provided the necessary information for determining the specific effects of fluid loading. Second, a theoretical model, which provides separation and evaluation of the effects of fluid loading, was developed for interpretation of the observed experimental results. The model, which was derived from general plate theory, predicts experimental results reasonably well and should apply to other similar systems.

EXPERIMENTAL APPARATUS

The experimental objectives were to provide data for determining the effectiveness of damping tiles for reducing vibration of plates in water and for determining the effects of the vibration-induced pressure field with respect to assessing the effectiveness of damping tiles.

The acceleration power spectral density of a point-excited, clamped-edge steel plate was measured in both air and water environments for both damped and undamped plates. To provide for theoretically modeling the experiment, the dimensions of the steel plate utilized in this experiment adequately satisfied the requirements of thin-plate theory. The thickness and material properties of the plate were also comparable to the plating that is used for ship construction.

Figure 1 shows the apparatus used to measure plate vibration response to a point-force excitation. A 2-ft by 3-ft by 1/4-in.-thick steel plate was clamped along each edge to a stiff, massive steel frame. The bolts of the vise mechanism were tightened with a torque wrench to maintain as uniform a clamping force as possible along the edges of the plate. To prevent twisting of the frame at its corners, the frame-plate unit was bolted into a plywood box. The entire assembly was then vibration isolated from its surroundings by suspending it on shock cord from an overhead chain hoist.

A more detailed view of the plate, edge-clamping mechanism, shaker, force gage, and accelerometers is shown in Fig. 2. An Endevco force gage (model 2103-500) was stud mounted to an adapter that was fastened to the plate by dental cement. A Wilcoxon electrodynamic reaction shaker (model F1), which excited the plate through a frequency range of 35-3000 Hz, was then

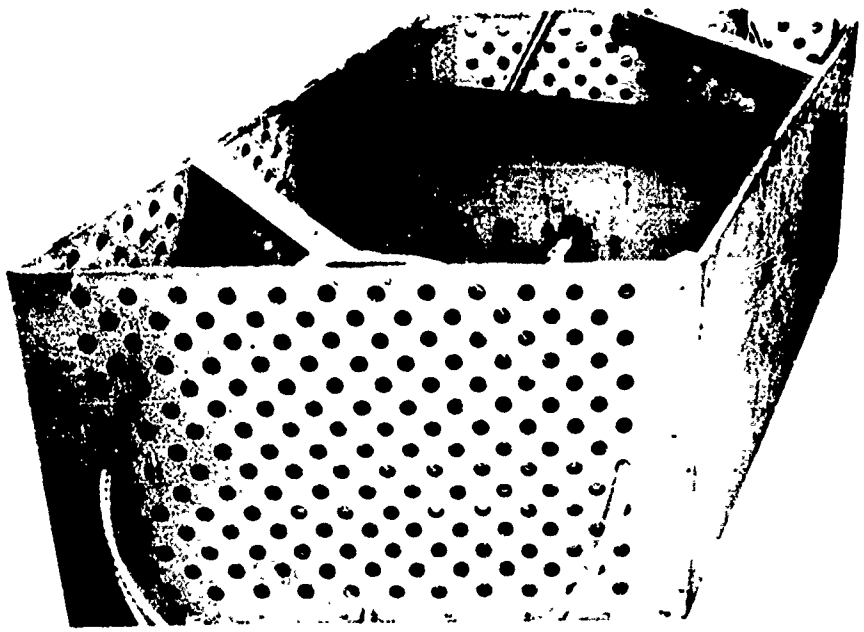

Fig. 1. Vibrating Plate Apparatus

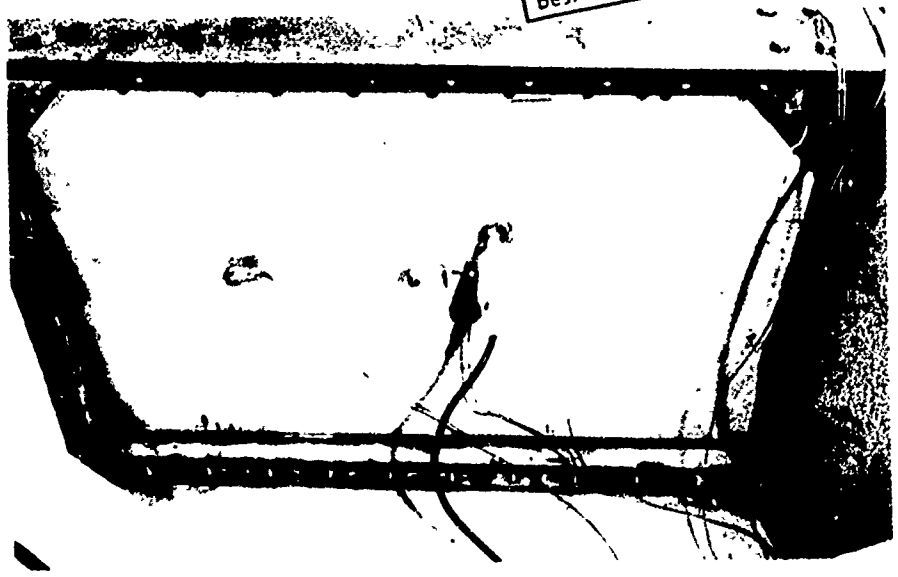

Fig. 2. Plate Detail -- Edge-Clamping Mechanism, Force Gage, Shaker, and Accelerometers

coupled to the force gage by a stud. The combined shaker and force gage were mounted at a point 0.3 ft to the right of the vertical centerline of the plate and 0.2 ft above the horizontal centerline.

Two Endevco accelerometers (model 2122D) were mounted by Allen screws to adapters fastened to the plate by dental cement. Both accelerometers were mounted on the horizontal centerline of the plate, one on the vertical centerline and one 0.75 ft to the left of the vertical centerline.

The shaker, force gage, and accelerometers were selected with respect to low mass, frequency response within the desired range, and availability. The combined shaker and force gage, including mounting studs and adapter, had a total weight of approximately 1 lb. The force gage had a sensitivity of 125 (±2%) peak-mV/peak-lb within the frequency range 35-3000 Hz. Each accelerometer, including its mounting stud and adapter, had a total weight of 0.037 lb and a sensitivity of 12.5 (±5%) peak-mV/peak-g within the frequency range 2-6000 Hz.

Monsanto damping tiles are shown bonded to the plate in Fig. 3. Standard shipboard techniques were used to apply the 1/2-in.-thick tiles to the plate by means of Carbolene Neoprene-Adhesive F-1. The tiles covered the entire surface area on the side of the plate opposite to that on which the shaker and accelerometers were mounted. (Monsanto tiles and Carbolene F-1 adhesive are the materials normally utilized for shipboard damping applications.)

In Fig. 4, the experimental apparatus is shown suspended by shock cord and immersed in the water test tank at the Naval Underwater Systems Center's New London laboratory. Inasmuch as vibration of a plate in water, unlike that of one in air, may radiate a large pressure field into the surrounding fluid, holes were drilled in a portion of the plywood box in an attempt to minimize reflections of the radiated pressure field back to the surfaces of the plate. In addition, the sides of the box not attached to the clamping frame were placed at a 20° angle to the plane of the plate. And because vibration of the plate may excite vibrations of the plywood box, causing unwanted acoustic radiation, it seemed desirable to mass load the plywood box in order to reduce its vibration amplitude; to this end, four small, massive lead weights were attached to the long sides and bottom of the box.

A block diagram of the analysis equipment used to obtain the normalized acceleration power spectral density of the plate is presented in Fig. 5. The shaker generated a sinusoidal force as a result of a sinusoidal voltage applied to the input. This input signal was then swept through the frequency range 35-3000 Hz.

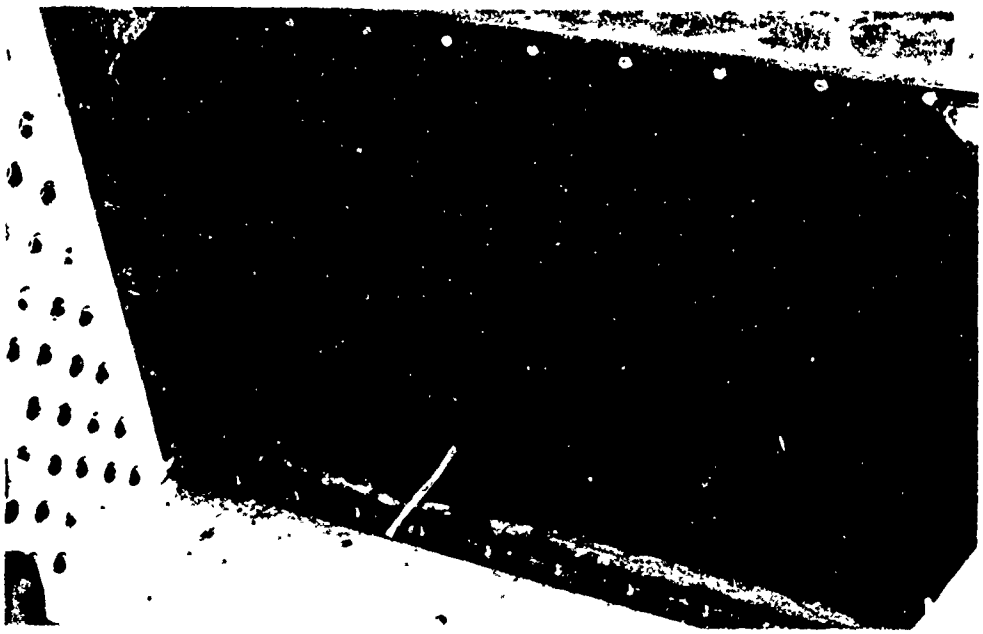

Fig. 3. Plate Detail — Damping-Tile Installation

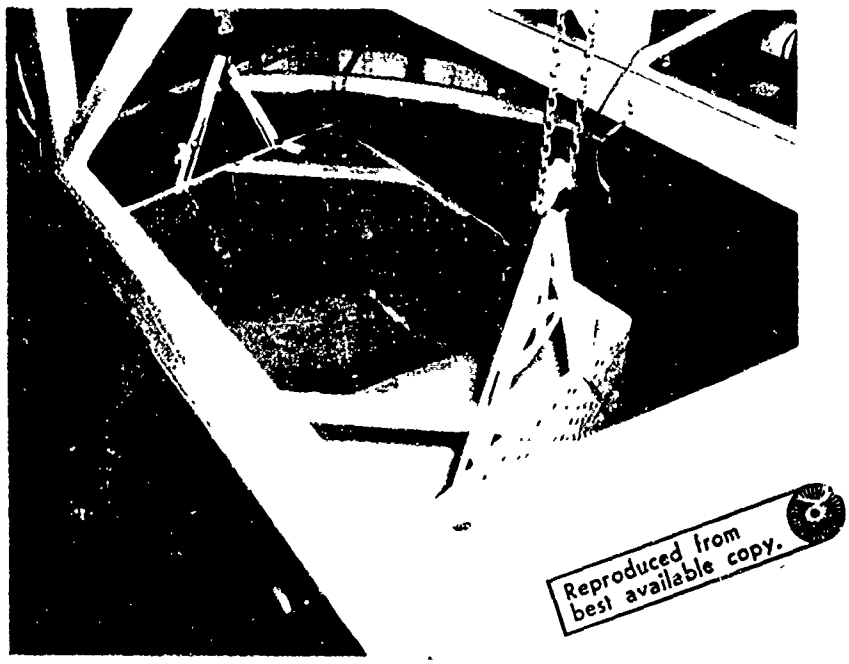

Fig. 4. Experimental Apparatus Immersed in Water

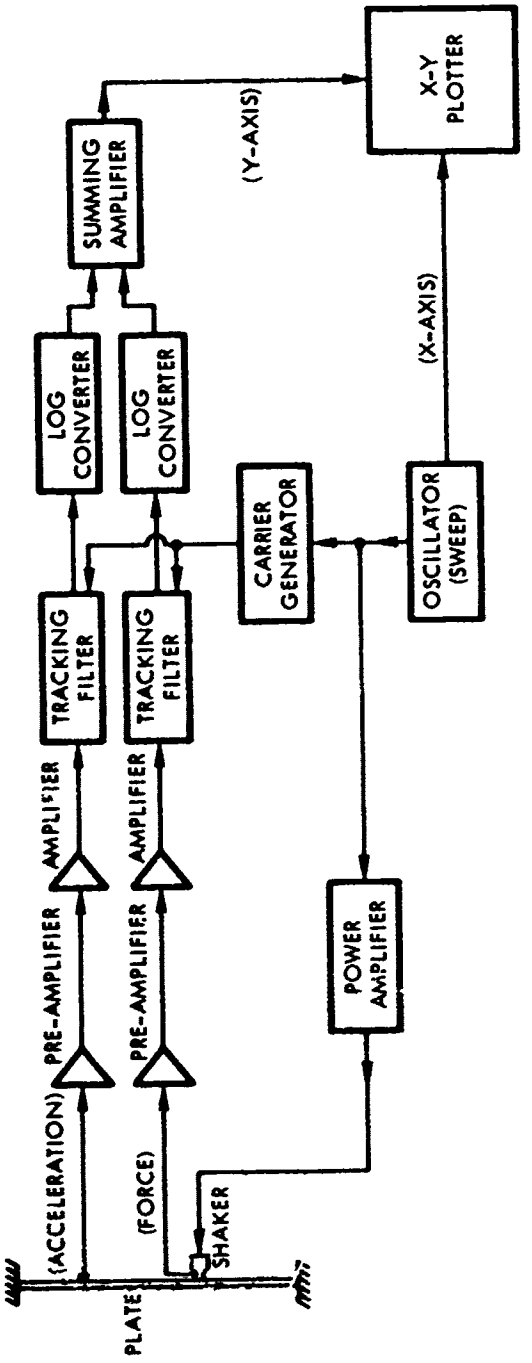

PLOTTER X-AXIS — LOG_{10} FREQUENCY
PLOTTER Y-AXIS — LOG_{10} ACCELERATION/FORCE

Fig. 5. Block Diagram of Analysis Equipment

The resulting voltage outputs from the force gage and one of the accelerometers were measured within 10-Hz bandwidths and fed to the indirect inputs of a summing amplifier. The ratio of the inputs, obtained via the summing amplifier, yielded a voltage output proportional to the plate-acceleration power spectral density that would result from a 1-lb force input. This normalized value was directly plotted versus frequency on an X-Y plotter.

THEORETICAL MODEL

As illustrated in Fig. 6, the theoretical model for this study consists of a finite plate, simply supported in an infinite, rigid baffle and immersed in a fluid of density ρ and speed of sound c. The plate is excited into motion by a pressure field $p(\underset{\sim}{x},t)$, where $\underset{\sim}{x} = (x,y)$. The resulting motion of the plate excites a secondary pressure field in the fluid on each side of the plate that, at the fluid-plate interface, also excites the plate. The secondary fields are indicated in Fig. 6 by $p_a(\underset{\sim}{x},0-,t)$ and $p_a(\underset{\sim}{x},0+,t)$.

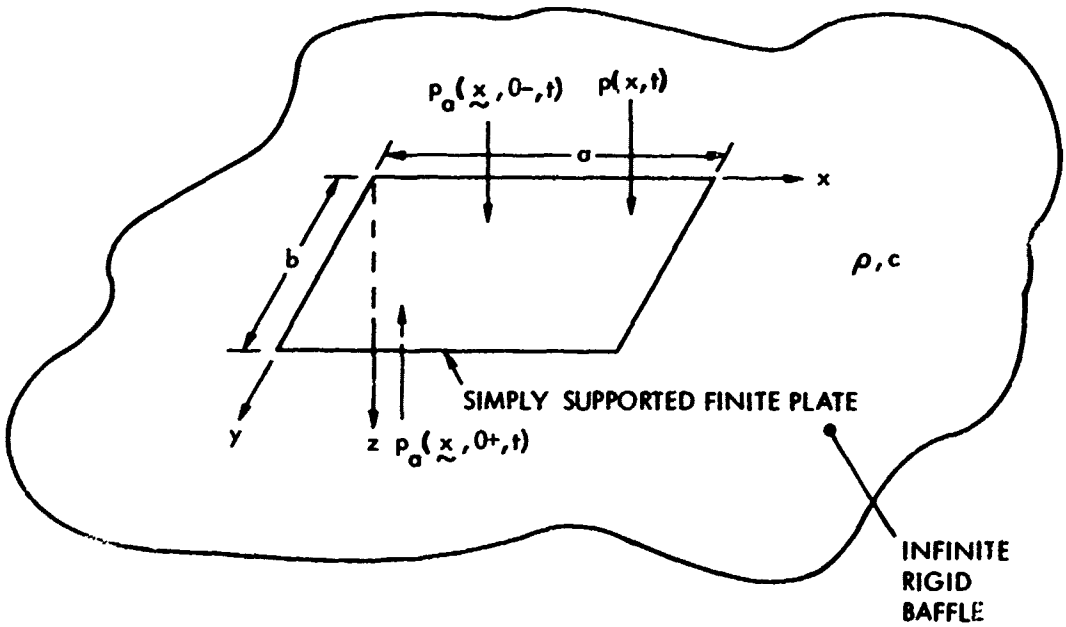

Fig. 6. Theoretical Model of Plate

Based on thin-plate theory, in which plate thickness is small compared with the plate bending wavelength, the equation governing the plate displacement $w(\underset{\sim}{x},t)$ in the z-coordinate direction is

$$D\nabla^4 w(\underset{\sim}{x},t) + r\frac{\partial w(\underset{\sim}{x},t)}{\partial t} + \mu\frac{\partial^2 w(\underset{\sim}{x},t)}{\partial t^2} = p(\underset{\sim}{x},t) + p_a(\underset{\sim}{x},0-,t) - p_a(\underset{\sim}{x},0+,t), \qquad (1)$$

where D is the plate's flexural rigidity, r is the damping per unit area, and μ is the mass per unit area of the plate.

The pressure field induced by the plate vibration is governed by the wave equation

$$\nabla^2 p_a(\underset{\sim}{x},z,t) = \frac{1}{c^2}\frac{\partial^2 p_a(\underset{\sim}{x},z,t)}{\partial t^2}, \qquad (2)$$

and the equation which then couples the induced pressure field to the plate motion is the linearized momentum equation

$$\left.\frac{\partial p_a(\underset{\sim}{x},z,t)}{\partial z}\right]_{z=\pm 0} = -\rho\frac{\partial^2 w(\underset{\sim}{x},t)}{\partial t^2}. \qquad (3)$$

In Eq. (1) it is assumed that the plate displacement can be determined in terms of the in vacuo normal modes $\alpha_{mn}(\underset{\sim}{x})$ by the equation[5]

$$w(\underset{\sim}{x},t) = \frac{1}{\sqrt{2\pi}}\int_{-\infty}^{\infty}\sum_{m,n=1}^{\infty} W_{mn}(\omega)\,\alpha_{mn}(\underset{\sim}{x})\exp(i\omega t)\,d\omega. \qquad (4)$$

The in vacuo normal modes are defined by

$$\alpha_{mn}(\underset{\sim}{x}) = \begin{cases} \frac{2}{\sqrt{ab}}\sin\frac{m\pi x}{a}\sin\frac{n\pi y}{b} & \text{for } (0,0) \le \underset{\sim}{x} \le (a,b) \\ 0 & \text{elsewhere.} \end{cases} \qquad (5)$$

Further, the in vacuo natural frequencies that correspond to these normal modes are defined by

$$\omega_{mn} = \sqrt{\frac{D}{\mu}}\, k_{mn}^2, \tag{6}$$

where

$$k_{mn}^2 = \left(\frac{m\pi}{a}\right)^2 + \left(\frac{n\pi}{b}\right)^2.$$

Because excitation forces on a ship's hull plating are usually random in nature, it is desirable to determine the response statistics of the vibrating structure. In the case of the finite plate, the normalized acceleration power spectral density was the plate statistic measured in the corresponding experimental study. The plate-acceleration power spectral density $\Phi_a(\underset{\sim}{x}, \omega)$ is related to the cross-spectral density of the exciting pressure field $S_{pp}(\underset{\sim}{x}, \underset{\sim}{\xi}', \omega)$ by the complex frequency response of the plate $H(\underset{\sim}{x}, \underset{\sim}{x}', \omega)$ in such a way that[6]

$$\Phi_a(\underset{\sim}{x}, \omega) = \omega^4 \iint_{-\infty}^{\infty} S_{pp}(\underset{\sim}{x}', \underset{\sim}{\xi}', \omega)\, H(\underset{\sim}{x}, \underset{\sim}{x}', -\omega)\, H(\underset{\sim}{x}, \underset{\sim}{x}'+\underset{\sim}{\xi}', \omega)\, d\underset{\sim}{\xi}'\, d\underset{\sim}{x}'. \tag{7}$$

The complex frequency response of the plate is defined by the equation

$$w(\underset{\sim}{x}, t) = H(\underset{\sim}{x}, \underset{\sim}{x}', \omega) \exp(i\omega t) \tag{8}$$

when

$$p(\underset{\sim}{x}, t) = \delta(\underset{\sim}{x}-\underset{\sim}{x}') \exp(i\omega t). \tag{9}$$

In order to solve Eq. (1) it is necessary to determine the induced pressure field $p_a(\underset{\sim}{x}, 0\pm, t)$ on both sides of the plate. By defining the Fourier transform pair

$$p_a(\underset{\sim}{x}, z, t) = \frac{1}{(2\pi)^{3/2}} \iint_{-\infty}^{\infty} P(\underset{\sim}{k}, z, \omega) \exp[i(\underset{\sim}{k} \cdot \underset{\sim}{x} + \omega t)]\, d\underset{\sim}{k}\, d\omega$$

$$P(\underset{\sim}{k}, z, \omega) = \frac{1}{(2\pi)^{3/2}} \iint_{-\infty}^{\infty} p_a(\underset{\sim}{x}, z, t) \exp\left[-i(\underset{\sim}{k} \cdot \underset{\sim}{x} + \omega t)\right] d\underset{\sim}{x}\, dt \tag{10}$$

and by imposing the radiation condition on $p_a(\underset{\sim}{x}, z, t)$ such that $p_a(\underset{\sim}{x}, z, t)$ must radiate away from the plate or $p_a(\underset{\sim}{x}, z, t)$ must decay with distance away from the plate, Eq. (2) becomes

$$P(\underset{\sim}{k}, z, \omega) = \begin{cases} P_1(\underset{\sim}{k}, \omega) \exp\left(-ik_o\sqrt{1 - (k/k_o)^2}\, z\right) & \text{for } |\underset{\sim}{k}| \le |k_o| \\ P_2(\underset{\sim}{k}, \omega) \exp\left(-\sqrt{k^2 - k_o^2}\, z\right) & \text{for } |\underset{\sim}{k}| > |k_o| \end{cases} \quad z \ge 0$$

and (11)

$$P(\underset{\sim}{k}, z, \omega) = \begin{cases} P_3(\underset{\sim}{k}, \omega) \exp\left(ik_o\sqrt{1 - (k/k_o)^2}\, z\right) & \text{for } |\underset{\sim}{k}| \le |k_o| \\ P_4(\underset{\sim}{k}, \omega) \exp\left(\sqrt{k^2 - k_o^2}\, z\right) & \text{for } |\underset{\sim}{k}| > |k_o| \end{cases} \quad z \le 0 .$$

In Eq. (11), $k_o = \omega/c$ and $k = \sqrt{k_1^2 + k_2^2} = |\underset{\sim}{k}|$. From Eqs. (3), (4), (10), and (11)

$$p_a(\underset{\sim}{x}, 0+, t) = \frac{1}{(2\pi)^{5/2}} \int_{-\infty}^{\infty} \sum_{q,s=1}^{\infty} \rho\omega^2 W_{qs}(\omega) \left\{ i \int_{|\underset{\sim}{k}| \le |k_o|} \frac{g_{qs}(\underset{\sim}{k}) \exp(i\underset{\sim}{k} \cdot \underset{\sim}{x})\, d\underset{\sim}{k}}{k_o\sqrt{1 - (k/k_o)^2}} - \int_{|\underset{\sim}{k}| > |k_o|} \frac{g_{qs}(\underset{\sim}{k}) \exp(i\underset{\sim}{k} \cdot \underset{\sim}{x})\, d\underset{\sim}{k}}{\sqrt{k^2 - k_o^2}} \right\} \exp(i\omega t)\, d\omega , \tag{12}$$

where

$$g_{mn}(\underset{\sim}{k}) = \int_{-\infty}^{\infty} \alpha_{mn}(\underset{\sim}{x}) \exp(-i\underset{\sim}{k} \cdot \underset{\sim}{x})\, d\underset{\sim}{x}$$

and

$$p_a(\underset{\sim}{x}, 0-, t) = -p_a(\underset{\sim}{x}, 0+, t) .$$

Then, from Eqs. (1), (4), (6), and (12),

$$\mu \sum_{q,s=1}^{\infty} \left[\omega_{qs}^2 - \omega^2 + i\frac{r\omega}{\mu}\right] W_{qs}(\omega)\, \alpha_{qs}(\underset{\sim}{x}) = F(\underset{\sim}{x},\omega) - \frac{2}{(2\pi)^2} \sum_{q,s=1}^{\infty} \rho\omega^2\, W_{qs}(\omega)$$

$$\cdot \left\{ i \int_{|\underset{\sim}{k}|\le|k_o|} \frac{g_{qs}(\underset{\sim}{k}) \exp\,(i\underset{\sim}{k}\cdot\underset{\sim}{x})\, d\underset{\sim}{k}}{k_o\sqrt{1-(k/k_o)^2}} - \int_{|\underset{\sim}{k}|>|k_o|} \frac{g_{qs}(\underset{\sim}{k}) \exp\,(i\underset{\sim}{k}\cdot\underset{\sim}{x})\, d\underset{\sim}{k}}{\sqrt{k^2-k_o^2}} \right\}, \tag{13}$$

where

$$F(\underset{\sim}{x},\omega) = \frac{1}{\sqrt{2\pi}} \int_{-\infty}^{\infty} p(\underset{\sim}{x},t) \exp\,(-i\omega t)\, dt\,; \tag{14}$$

Multiplying Eq. (13) by $\alpha_{mn}(\underset{\sim}{x})$ and integrating over all $\underset{\sim}{x}$ yield

$$\left[\omega_{mn}^2 - \omega^2 + i\frac{r\omega}{\mu}\right] W_{mn}(\omega) + \frac{2}{(2\pi)^2\mu} \sum_{q,s=1}^{\infty} \rho\omega^2\, W_{qs}(\omega)$$

$$\cdot \left\{ i \int_{|\underset{\sim}{k}|\le|k_o|} \frac{g_{mn}(-\underset{\sim}{k})\, g_{qs}(\underset{\sim}{k})\, d\underset{\sim}{k}}{k_o\sqrt{1-(k/k_o)^2}} - \int_{|\underset{\sim}{k}|>|k_o|} \frac{g_{mn}(-\underset{\sim}{k})\, g_{qs}(\underset{\sim}{k})\, d\underset{\sim}{k}}{\sqrt{k^2-k_o^2}} \right\} = \frac{F_{mn}(\omega)}{\mu}, \tag{15}$$

where

$$F_{mn}(\omega) = \int_{-\infty}^{\infty} F(\underset{\sim}{x},\omega)\, \alpha_{mn}(\underset{\sim}{x})\, d\underset{\sim}{x}\,. \tag{16}$$

Define

$$r_{mnqs}(\omega) = \frac{2\rho\omega}{(2\pi)^2} \int_{|\underset{\sim}{k}|\le|k_o|} \frac{g_{mn}(-\underset{\sim}{k})\, g_{qs}(\underset{\sim}{k})\, d\underset{\sim}{k}}{k_o\sqrt{1-(k/k_o)^2}} \tag{17}$$

and

$$\mu_{mnqs}(\omega) = \frac{2\rho}{(2\pi)^2} \int_{|\underset{\sim}{k}|>|k_o|} \frac{g_{mn}(-\underset{\sim}{k})\, g_{qs}(\underset{\sim}{k})\, d\underset{\sim}{k}}{\sqrt{k^2 - k_o^2}}; \tag{18}$$

by substituting Eqs. (17) and (18) into Eq. (15), one obtains the following set of coupled equations for the frequency-dependent, modal coefficients of the plate motion $W_{mn}(\omega)$:

$$\sum_{q,s=1}^{\infty} \left\{ \left[\delta_{mq}\, \delta_{ns}\, \omega_{mn}^2 - \omega^2 \left(\delta_{mq}\, \delta_{ns} + \frac{\mu_{mnqs}(\omega)}{\mu} \right) \right] + \left[i\frac{r\omega}{\mu} \left(\delta_{mq}\, \delta_{ns} + \frac{r_{mnqs}(\omega)}{r} \right) \right] \right\} \tag{19}$$

$$\cdot\, W_{qs}(\omega) = \frac{F_{mn}(\omega)}{\mu},$$

where

$$\delta_{ij} = \begin{cases} 1 & i=j \\ 0 & i \neq j \end{cases}.$$

Equation (19) represents the solution for $W_{qs}(\omega)$ in terms of an infinite $m \times n$ set of simultaneous equations. In these equations $\mu_{mnqs}(\omega)$ appears as an additional inertial term and $r_{mnqs}(\omega)$ as an additional resistive term. Both terms occur as a result of fluid loading and introduce cross coupling of the m,n-th mode to the q,s-th mode. If both μ_{mnqs} and r_{mnqs} were zero, Eq. (19) would reduce to the in vacuo uncoupled solution of $W_{mn}(\omega)$.

Consider the fluid-loading solution for $W_{qs}(\omega)$ in Eq. (19). By defining

$$A_{mnqs}(\omega) = \left[\delta_{mq}\, \delta_{ns}\, \omega_{mn}^2 - \omega^2 \left(\delta_{mq}\, \delta_{ns} + \frac{\mu_{mnqs}(\omega)}{\mu} \right) \right] + i\left[\frac{r\omega}{\mu} \left(\delta_{mq}\, \delta_{ns} + \frac{r_{mnqs}(\omega)}{r} \right) \right], \tag{20}$$

Eq. (19) becomes

$$\sum_{q,s=1}^{\infty} A_{mnqs}(\omega)\, W_{qs}(\omega) = \frac{F_{mn}(\omega)}{\mu} . \tag{21}$$

By also defining $B_{mnqs}(\omega)$ in such a way that

$$\sum_{k,\ell=1}^{\infty} B_{ijk\ell}\, A_{k\ell mn} = \delta_{im}\, \delta_{jn} , \tag{22}$$

Eqs. (21) and (22) may be utilized to show that

$$W_{mn}(\omega) = \frac{1}{\mu} \sum_{q,s=1}^{\infty} B_{mnqs}(\omega)\, F_{qs}(\omega) . \tag{23}$$

From the definition in Eqs. (8) and (9) of the complex frequency response, Eqs. (4), (14), (16), and (23) may be utilized to obtain the fluid-loaded plate's complex frequency response

$$H(\underset{\sim}{x}, \underset{\sim}{x}', \omega) = \frac{1}{\mu} \sum_{m,n=1}^{\infty} \sum_{q,s=1}^{\infty} B_{mnqs}(\omega)\, \alpha_{mn}(\underset{\sim}{x})\, \alpha_{qs}(\underset{\sim}{x}') . \tag{24}$$

From Eqs. (7) and (24), one can express the fluid-loaded plate's acceleration power spectral density as

$$\Phi_a(\underset{\sim}{x}, \omega) = \frac{\omega^4}{\mu^2} \sum_{i,j=1}^{\infty} \sum_{k,\ell=1}^{\infty} \sum_{m,n=1}^{\infty} \sum_{q,s=1}^{\infty} \alpha_{ij}(\underset{\sim}{x})\, \alpha_{mn}(\underset{\sim}{x})\, B_{ijk\ell}(-\omega)\, B_{mnqs}(\omega)$$

$$\cdot \iint_{-\infty}^{\infty} S_{pp}(\underset{\sim}{x}', \underset{\sim}{\xi}', \omega)\, \alpha_{k\ell}(\underset{\sim}{x}')\, \alpha_{qs}(\underset{\sim}{x}' + \underset{\sim}{\xi}')\, d\underset{\sim}{x}'\, d\underset{\sim}{\xi}' . \tag{25}$$

The cross-spectral density $S_{pp}(\underset{\sim}{x}', \underset{\sim}{\xi}', \omega)$ of the excitation force is given by

$$S_{pp}(\underset{\sim}{x}', \underset{\sim}{\xi}', \omega) = \delta(\underset{\sim}{x}' - \underset{\sim}{x}_o)\ \delta(\underset{\sim}{x}' + \underset{\sim}{\xi}' - \underset{\sim}{x}_o) \tag{26}$$

for a sinusoidal excitation force of unit amplitude over all ω applied at a point $\underset{\sim}{x}_o$.

This expression for excitation force was chosen because it corresponds most closely to that of the experimental analysis.

Substitution of Eq. (26) into Eq. (25) and integration over $\underset{\sim}{x}'$ and $\underset{\sim}{\xi}'$ yield the acceleration power spectral density for a point-excited, fluid-loaded finite plate, which is

$$\Phi_a(\underset{\sim}{x}, \omega) = \frac{\omega^4}{\mu^2} \sum_{i,j=1}^{\infty} \sum_{k,\ell=1}^{\infty} \sum_{m,n=1}^{\infty} \sum_{q,s=1}^{\infty} B_{ijk\ell}(-\omega)\, B_{mnqs}(\omega)\, \alpha_{ij}(\underset{\sim}{x})\, \alpha_{mn}(\underset{\sim}{x}) \cdot \alpha_{k\ell}(\underset{\sim}{x}_o)\, \alpha_{qs}(\underset{\sim}{x}_o)\ . \tag{27}$$

Now, consider the in vacuo solution for the acceleration power spectral density. By substituting Eq. (19), with $r_{mnqs} = \mu_{mnqs} = 0$, into Eq. (22), one obtains

$$B_{ijmn}(\omega) = \frac{\delta_{im}\, \delta_{jn}}{\left[\omega_{mn}^2 - \omega^2 + i\,\frac{r\omega}{\mu}\right]}\ . \tag{28}$$

Substitution of Eq. (28) into Eq. (27) gives

$$\Phi_a(\underset{\sim}{x}, \omega) = \frac{\omega^4}{\mu^2} \sum_{k,\ell=1}^{\infty} \sum_{q,s=1}^{\infty} \frac{\alpha_{k\ell}(\underset{\sim}{x})\, \alpha_{qs}(\underset{\sim}{x})\, \alpha_{k\ell}(\underset{\sim}{x}_o)\, \alpha_{qs}(\underset{\sim}{x}_o)}{\left[\omega_{k\ell}^2 - \omega^2 - i\,\frac{r\omega}{\mu}\right]\left[\omega_{qs}^2 - \omega^2 + i\,\frac{r\omega}{\mu}\right]}, \tag{29}$$

which is the point-excited, in vacuo solution for the acceleration power spectral density.

EXPERIMENTAL RESULTS

Figures 7 and 8 are comparisons of measured, normalized acceleration power spectral densities of point-excited, clamped-edge damped and undamped plates in an air environment. Figures 9 and 10 are comparisons of measured, normalized acceleration power spectral densities of the same plates in a water environment. The acceleration spectra of Figs. 7 and 9 were measured at the center of the plate ($x = 1.5$ ft, $y = 1.0$ ft) and those of Figs. 8 and 10 were measured at a point along the horizontal centerline midway between the center and edge of the plate ($x = 2.25$ ft, $y = 1.0$ ft). (See Figs. 2 and 6.)

Figures 7, 8, 9, and 10 indicate that the application of damping tiles is accompanied by a reduction in the peak acceleration levels of the plate. However, comparison of Figs. 7 and 9 also shows that, for identical plates, the reduction is less for water loading than for air loading. Similarly, except for frequencies greater than 1500 Hz, comparison of Figs. 8 and 10 also shows less reduction for water loading. It appears, therefore, that damping tiles are less effective in water than in air for reducing plate vibrations; inasmuch as identical plates and tiles were used in air and water, the water environment must cause the reduction in effectiveness.

To understand the smaller reduction of plate acceleration levels observed for water loading, one must determine the extent to which the reduction in water is governed by the properties of the damping tile in comparison with that portion governed by the properties of water. This will be accomplished by utilizing the theory developed in the preceding section to describe the major effects of water loading. A theoretical analysis will then be developed to quantitatively interpret the separate effects of water loading and damping-tile applications on reducing plate vibration.

WATER LOADING

To illustrate the effects of water loading, Fig. 11 presents a comparison of computed air- and water-loaded plate-acceleration spectra at the center of an undamped plate. These spectra were computed by numerical evaluation of Eqs. (27) and (29).* Only the first few corresponding natural frequencies

*Equation (29) describes the acceleration of a plate in vacuo, but because the density of air is small, Eq. (29) is considered valid for the acceleration of a plate in air.

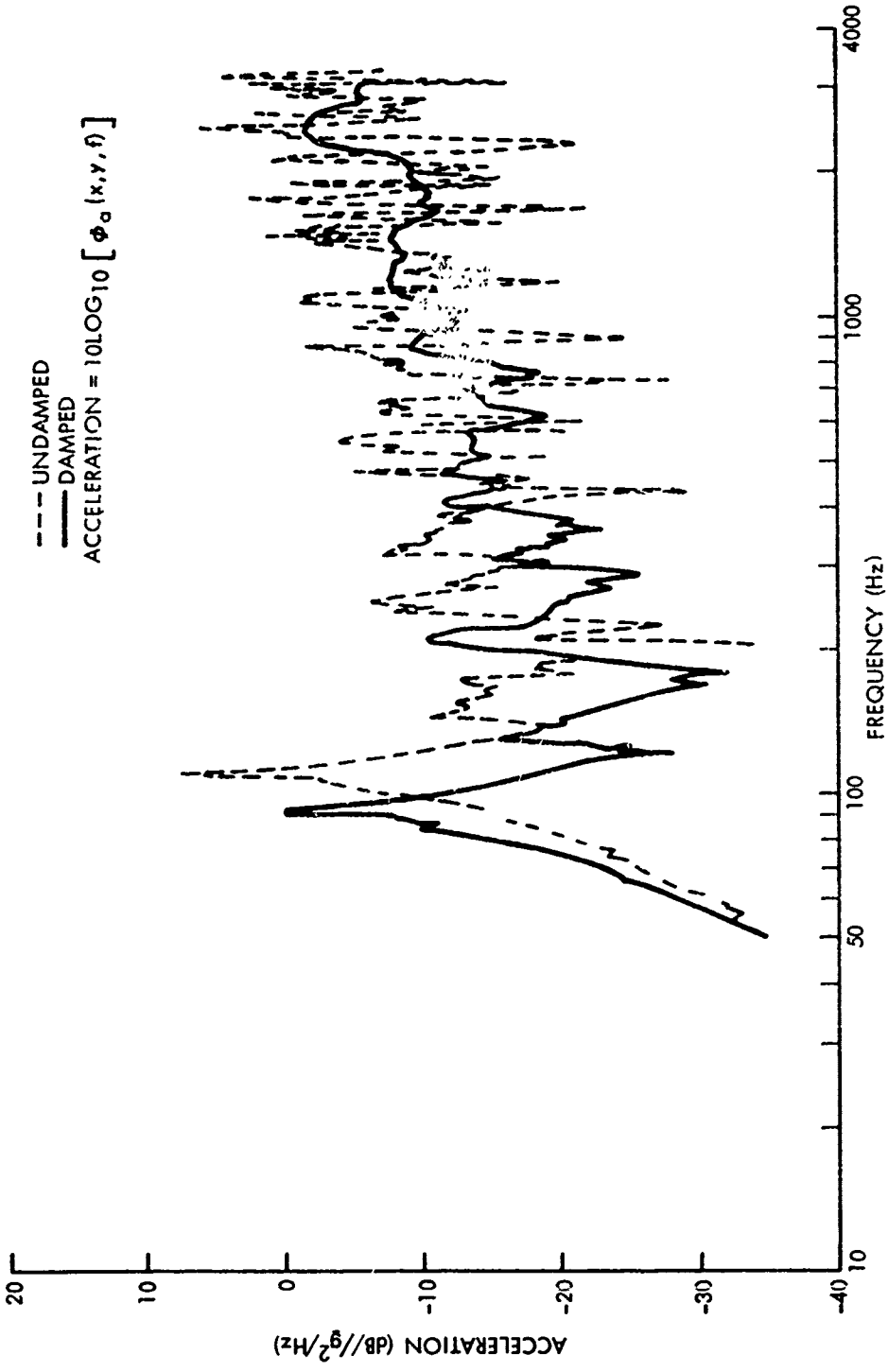

Fig. 7. Measured Acceleration Spectra of Damped and Undamped Air-Loaded Plates (at x = 1.5 ft, y = 1.0 ft)

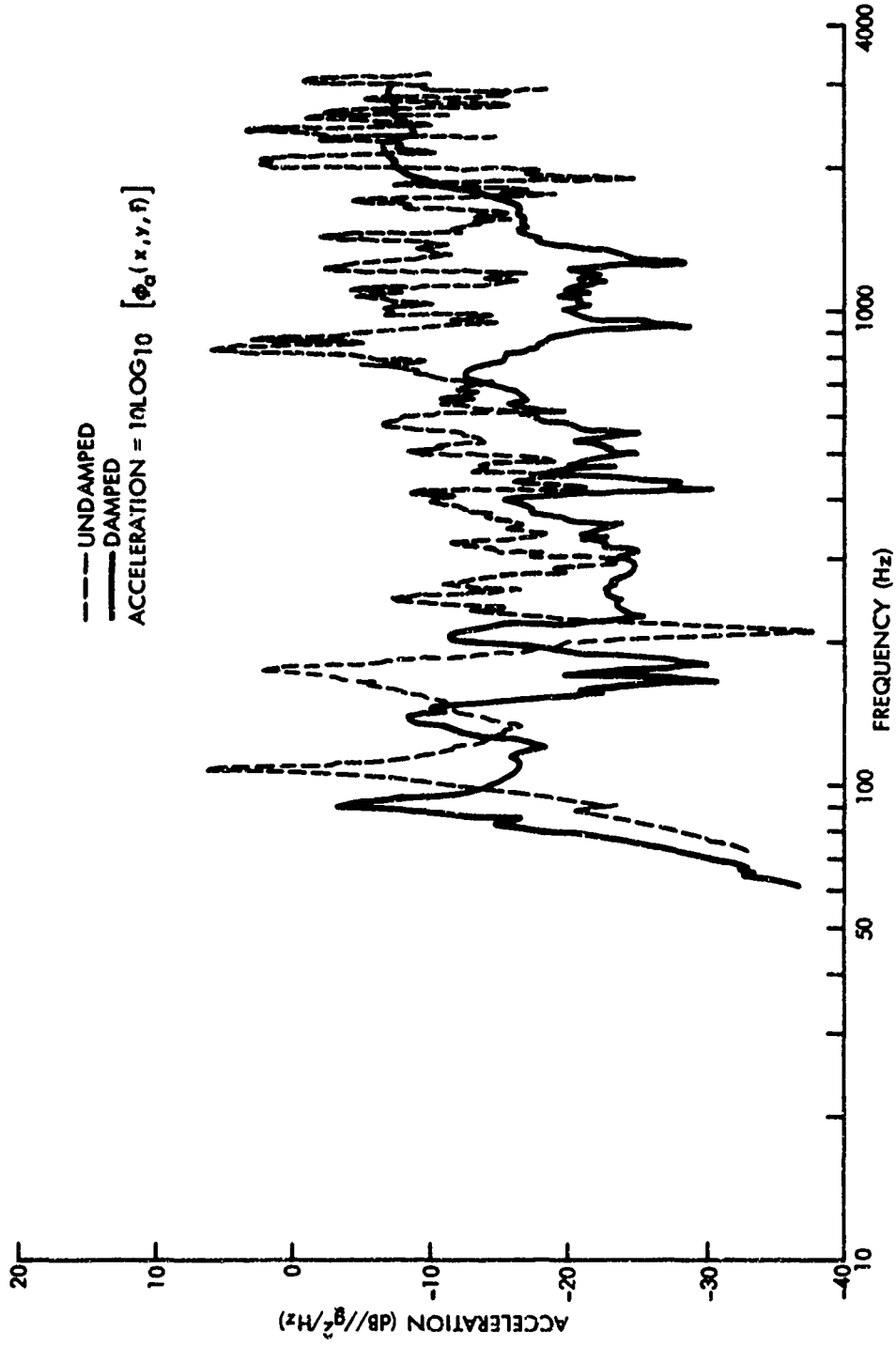

Fig. 8. Measured Acceleration Spectra of Damped and Undamped Air-Loaded Plates (at x = 2.25 ft, y = 1.0 ft)

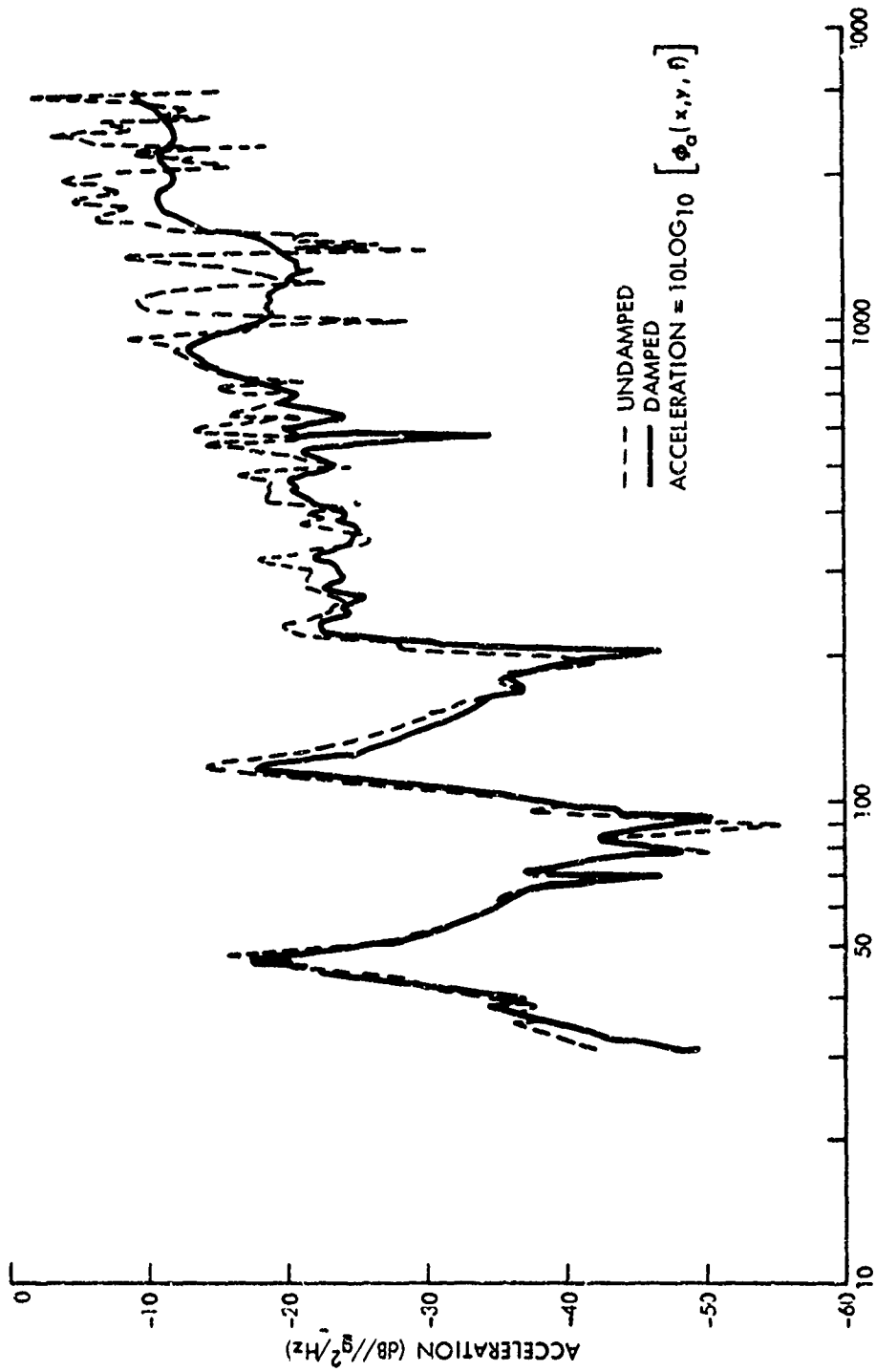

Fig. 9. Measured Acceleration Spectra of Damped and Undamped Water-Loaded Plates (at x = 1.5 ft, y = 1.0 ft)

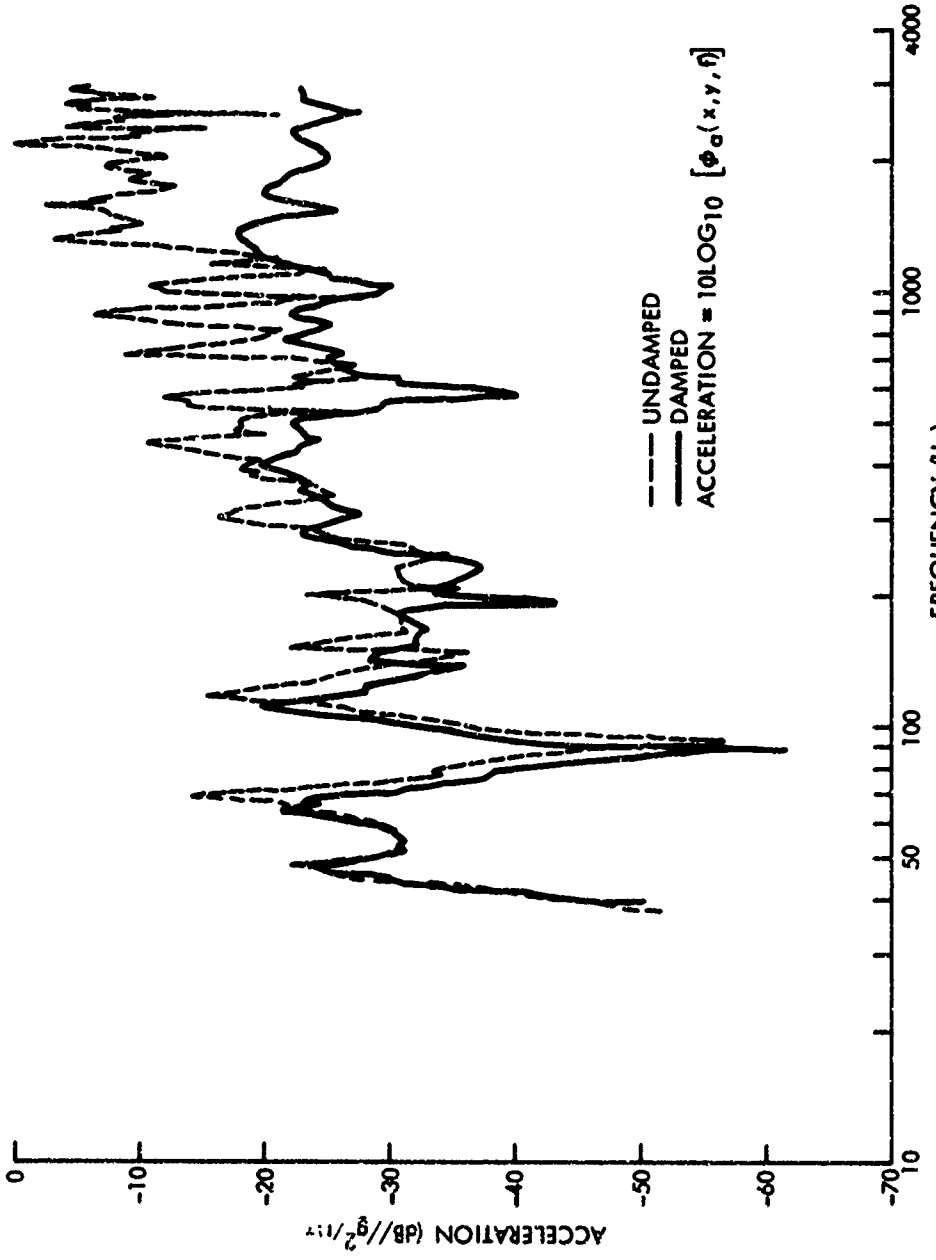

Fig. 10. Measured Acceleration Spectra of Damped and Undamped Water-Loaded Plates (at x = 2.25 ft, y = 1.0 ft)

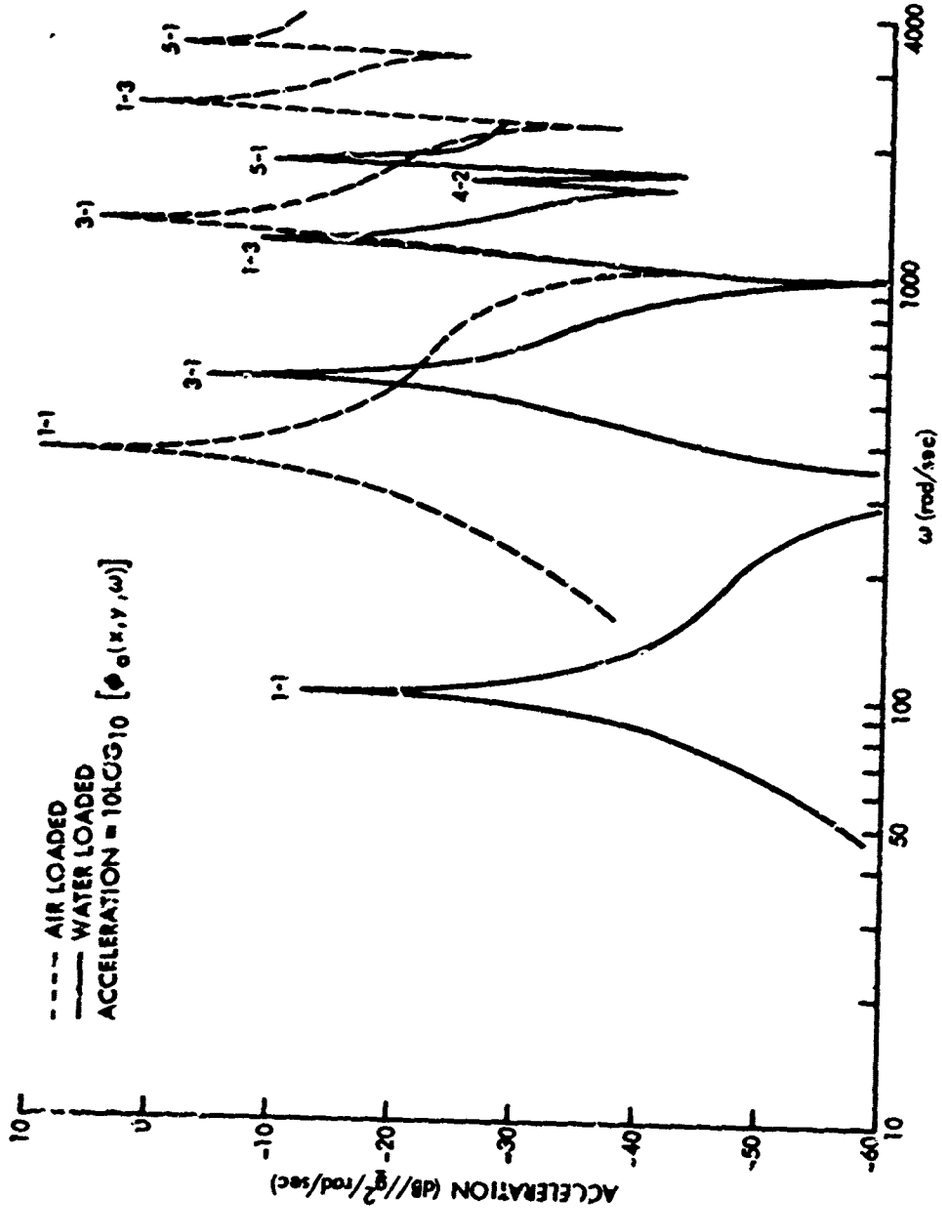

Fig. 11. Computed Acceleration Spectra of Undamped Air- and Water-Loaded Plates (at x = 1.5 ft, y = 1.0 ft)

between air- and water-loaded plates* are presented because of computational difficulties encountered for a water-loaded plate at high frequencies. The plate natural frequencies at which resonance occurs, are identified in Fig. 11 by their mode numbers. For convenience, the plate damping is assumed to be 1 percent of the in vacuo critical value for both air- and water-loaded plates (where the in vacuo critical damping for a finite plate is defined as $r_c = 2\mu\omega_{mn}$). This damping value is comparable to that computed from the Q, or sharpness of resonance of the measured spectrum shown in Fig. 9 for the undamped air-loaded plate.

The major effects of water loading evidenced by the spectra of Fig. 11 are

- a reduction in natural frequencies,
- a decrease in the general levels of acceleration, and
- a similarity in the sharpness of resonance Q.

To express these effects quantitatively, the equations on which the spectral computations were based will be investigated in conjunction with the computed spectra of Fig. 11.

The dependence of the air-loaded plate-acceleration spectrum on the properties of the plate is evident in Eq. (29). In Eq. (27), however, the dependence of a water-loaded plate-acceleration spectrum on the properties of both plate and water is not clear. This difference between the spectral equations for air- and water-loaded plates is a result of cross coupling between plate motion and the surrounding water; this cross coupling is introduced into the water-loaded plate equation via the fluid mass μ_{mnqs} and the fluid damping r_{mnqs}. Therefore, to understand the dependence of plate motion on the water environment, it is necessary to determine the magnitudes of mass and damping associated with the water relative to those of the plate alone.

Table 1 lists the computed natural frequencies for the water-loaded plate spectrum of Fig. 11 and the corresponding estimated natural frequencies.

*Figure 11, however, does not display a one-to-one correspondence between air- and water-loaded plate resonances. Cross coupling of the plate motion to the water causes a change in mode shape between corresponding air- and water-loaded plate modes. For certain modes, a change in shape is accompanied by a spatial shift in the nodal lines. Consequently, acceleration excitation at a nodal line for air loading may produce a resonance for water loading.

Table 1

COMPUTED AND ESTIMATED NATURAL FREQUENCIES

Mode No. m-n	Air Loading ω_{mn}	μ_{mnmn}	Water Loading ω'_{mn}	
			Estimated	Computed
1-1	377.5	3.970	102.6	102.5
2-1	725.9	1.973	270.1	269.9
1-2	1161	1.574	475.4	475.6
3-1	1307	1.466	550.7	562.2
2-2	1510	1.265	675.9	674.8
3-2	2091	1.030	1014	1016
4-1	2120	1.057	1018	1026
1-3	2468	1.148	1148	1194
2-3	2816	0.905	1434	1435
4-2	3904	0.854	1511	1512
5-1	3165	0.870	1635	1659
3-3	3397	0.804	1807	1814
5-2	3949	0.722	2181	2185
Plate Properties: $\mu = 0.317$ lb-sec^2/ft^3 and D = 3575 lb-ft				

Since plate natural frequencies are proportional to $\mu^{-1/2}$, the water-loaded natural frequencies were estimated by utilizing only the autocoupled fluid mass μ_{mnmn} and the mass of the plate. That is,

$$\frac{\omega'_{mn}}{\omega_{mn}} = \left[\frac{\mu}{\mu + \mu_{mnmn}}\right]^{1/2}, \tag{30}$$

where ω'_{mn} is the estimated water-loading natural frequency. The computed and estimated natural frequencies differ, on the average, by less than 1 percent; therefore the reduction in natural frequencies accompanying water loading is due almost entirely to the autocoupled fluid mass μ_{mnmn}.

To resolve the coupling properties of the fluid damping r_{mnqs}, an attempt was made to predict the resonance amplitudes by using only the autocoupled resistive term r_{mnmn}. However, predictions based only on r_{mnmn} were not in agreement with the actual spectral computations shown in Fig. 11. Consequently, it was concluded that fluid damping associated with a particular mode (r'_{mn}) is a summation of many contributions of r_{mnqs}. Because of this extensive cross coupling of fluid damping terms, it is difficult to quantitatively evaluate the resistive component of water loading.

To circumvent this difficulty, it is hypothesized that an equivalent, uncoupled expression for the water-loading acceleration power spectral density of Eq. (27) might be written

$$\Phi_a(\underset{\sim}{x}, \omega) = \frac{\omega^4}{\mu^2} \sum_{m,n=1}^{\infty} \sum_{q,s=1}^{\infty} \alpha_{mn}(\underset{\sim}{x})\, \alpha_{mn}(\underset{\sim}{x}_o)\, \alpha_{qs}(\underset{\sim}{x})\, \alpha_{qs}(\underset{\sim}{x}_o)$$

$$\cdot \frac{1}{\left\{\left[\omega_{mn}^2 - \omega^2\left(1 + \frac{\mu_{mnmn}}{\mu}\right)\right] - i\left[\frac{r\omega}{\mu}\left(1 + \frac{r'_{mn}}{r}\right)\right]\right\}\left\{\left[\omega_{qs}^2 - \omega^2\left(1 + \frac{\mu_{qsqs}}{\mu}\right)\right] + i\left[\frac{r\omega}{\mu}\left(1 + \frac{r'_{qs}}{r}\right)\right]\right\}} \cdot \tag{31}$$

where μ_{mnmn}, based on Eq. (30), is the fluid mass, and r'_{mn} is the equivalent fluid damping. In Eq. (31) for the water-loaded plate spectrum and Eq. (29) for the air-loaded plate spectrum, one may show that near a particular resonance (i,j) the maximum and controlling term in the summation occurs when $m = q = i$ and $n = s = j$. This assumption, however, is valid only when the

total damping $(r + r'_{mn})$ of the vibrating system is less than 10 percent of the in vacuo critical value r_c.* When this condition is satisfied, the acceleration power spectral densities in the vicinity of the i, j-th resonance for both water- and air-loaded plates, respectively, may be approximated by

$$\Phi_{a\,ij}(\underset{\sim}{x}, \omega) = \frac{\omega^4}{\mu^2} \frac{\alpha^2_{ij}(\underset{\sim}{x})\, \alpha^2_{ij}(\underset{\sim}{x}_o)}{\left\{\left[\omega^2_{ij} - \omega^2\left(1 + \frac{\mu_{ijij}(\omega)}{\mu}\right)\right]^2 + \left[\frac{r\omega}{\mu}\left(1 + \frac{r'_{ij}(\omega)}{r}\right)\right]^2\right\}} \tag{32}$$

and

$$\Phi_{a\,ij}(\underset{\sim}{x}, \omega) = \frac{\omega^4}{\mu^2} \frac{\alpha^2_{ij}(\underset{\sim}{x})\, \alpha^2_{ij}(\underset{\sim}{x}_o)}{\left[\left(\omega^2_{ij} - \omega^2\right)^2 + \left(\frac{r\omega}{\mu}\right)^2\right]}. \tag{33}$$

For brevity, water-loading quantities will hereafter be denoted by primes, such as $\Phi'_{a\,ij}$.

Equations (32) and (33) can be utilized to quantitatively evaluate the reduction in resonance amplitudes and any change in sharpness of resonance that accompanies water loading. The resonance amplitude for a water-loaded plate is evaluated by letting $\omega = \omega'_{ij}$ in Eq. (32); that is

$$\Phi'_{a\,ij}(\underset{\sim}{x}, \omega'_{ij}) = \frac{Dk^4_{ij}\, \alpha^2_{ij}(\underset{\sim}{x})\, \alpha_{ij}(\underset{\sim}{x}_o)}{\left[\mu + \mu_{ijij}(\omega'_{ij})\right]\left[r + r'_{ij}(\omega'_{ij})\right]^2}. \tag{34}$$

For an air-loaded plate, the resonance amplitude may be determined by letting $\omega = \omega_{ij}$ in Eq. (33), or

$$\Phi_{a\,ij}(\underset{\sim}{x}, \omega_{ij}) = \frac{Dk^4_{ij}\, \alpha^2_{ij}(\underset{\sim}{x})\, \alpha^2_{ij}(\underset{\sim}{x}_o)}{\mu r^2}. \tag{35}$$

*This limitation imposed on the magnitude of total damping is dependent on the frequency density of resonance modes and the magnitude of μ_{ijij}.

The sharpness of resonance Q is defined as the resonance frequency ω_{mn} divided by the half-power-point bandwidth of the resonance peak $\Delta\omega_{mn}$. From Eqs. (32) and (33), for water loading,

$$Q'_{ij}(\underset{\sim}{x}, \omega'_{ij}) = \frac{\omega'_{ij}}{\Delta\omega'_{ij}} \cong \sqrt{D}\, k_{ij}^2 \left\{ \frac{\sqrt{\mu + \mu_{ijij}(\omega'_{ij})}}{r + r'_{ij}(\omega'_{ij})} \right\} = \frac{1}{2\zeta} \left[\frac{\sqrt{1 + \dfrac{\mu_{ijij}(\omega'_{ij})}{\mu}}}{\left(1 + \dfrac{r'_{ij}(\omega'_{ij})}{r}\right)} \right], \quad (36)$$

and, for air loading,

$$Q_{ij}(\underset{\sim}{x}, \omega_{ij}) = \frac{\omega_{ij}}{\Delta\omega_{ij}} \cong \sqrt{D}\, k_{ij}^2 \left[\frac{\sqrt{\mu}}{r} \right] = \frac{1}{2\zeta}, \quad (37)$$

where ζ is defined as the fraction of in vacuo critical damping

$$\zeta = \frac{r}{r_c}. \quad (38)$$

Equations (34) and (36) indicate that both the resonance amplitude and the sharpness of resonance of water-loaded plates are functions of the autocoupled fluid mass μ_{ijij} and the equivalent fluid damping r'_{ij}. Table 1 shows that autocoupled mass is large compared with the mass of the plate. To determine how much the equivalent fluid damping r'_{ij} influences the water-loaded plate-acceleration spectra, Eqs. (34), (35), (36), and (37) were compared with the computed spectra in Fig. 11.

If the equivalent fluid damping r'_{mn} were negligible, the water-loaded plate resonance amplitudes would be lower than those of the corresponding air-loaded plate by an amount equal to $1 + (\mu_{ijij}/\mu)$. Further, the resonances would be sharper for water loading than for air loading by an amount equal to $\sqrt{1 + (\mu_{ijij}/\mu)}$. However, Fig. 11 and the values of μ_{ijij} listed in Table 1 reveal that resonances associated with water-loaded plate spectra are actually lower in height and broader in width than those predicted by mass considerations alone from Eqs. (34), (35), (36), and (37). One may conclude that the equivalent fluid damping r'_{mn} is not negligible compared with the plate damping.

Table 2 lists the computed values of plate damping r_s, autocoupled fluid damping r_{ijij}, and the equivalent fluid damping r'_{ij} for the resonances in

Table 2

PLATE, AUTOCOUPLED-FLUID, AND EQUIVALENT-FLUID DAMPING

Mode No. m-n	r	r_{mnmn}	r'_{mn}
1-1	2.39	5.29	5.53
3-1	8.27	17.45	2.36
1-3	15.65	76.40	9.10
3-3	21.55	17.80	5.38

Fig. 11. The values of equivalent fluid damping r'_{ij} were computed by utilizing Eq. (35), the water-loaded plate-acceleration spectra in Fig. 11, and the values of μ_{ijij} listed in Table 1. A comparison of r'_{ij} and r reveals that the equivalent fluid damping and plate damping are generally about the same order of magnitude. A comparison of r'_{ij} and the autocoupled fluid damping r_{ijij} reveals a wide variation in their magnitudes at each resonance. Although it is not known how the cross-coupled damping terms $r_{ijk\ell}$ combine to produce an equivalent damping r'_{ij}, the wide variation between r'_{ij} and r_{ijij} reinforces the hypothesis that the value of r'_{ij} is a result of many contributions of $r_{ijk\ell}$.

TILE DAMPING

The approximate theory (Eqs. (34) and (35)) developed to evaluate quantitatively the effects of water loading can also be utilized to understand the reduction in plate acceleration at resonance that accompanies the application of damping tiles. Tile applications increase the flexural rigidity, mass, and damping of a plate. However, the flexural rigidity of damping tile is only about 15 percent of that of the plate; therefore any increase in the flexural rigidity of the plate due to tile application can be considered negligible. Further, the mass of a damped plate can be expressed as the sum of the plate mass μ and the damping-tile mass μ_T. But the total damping of a plate can not be expressed in terms of the sum of the individual damping coefficients of the plate and the tile; hence the damping coefficient of the damped plate is denoted by r_d.

Consequently, from Eqs. (34) and (35), the ratios of acceleration amplitudes at corresponding resonances for damped and undamped plates may be written

$$\Phi_a(\omega_{ij})/\Phi_{ad}(\omega_{ijd}) = \left[\frac{\mu + \mu_T}{\mu}\right]\left[\frac{r_d(\omega_{ijd})}{r(\omega_{ij})}\right]^2 \tag{39}$$

and

$$\Phi'_a(\omega'_{ij})/\Phi'_{ad}(\omega'_{ijd}) = \left[\frac{\mu + \mu_T + \mu_{ijij}(\omega'_{ijd})}{\mu + \mu_{ijij}(\omega'_{ij})}\right]\left[\frac{r_d + r'_{ij}(\omega'_{ijd})}{r + r'_{ij}(\omega'_{ij})}\right]^2 , \tag{40}$$

where the subscript d denotes a quantity associated with the damped plate and, from Eqs. (6) and (30),

$$\omega_{ijd} = \sqrt{\frac{D}{\mu + \mu_T}}\, k_{ij}^2 \tag{41}$$

and

$$\omega'_{ijd} = \omega_{ijd}\Big/\sqrt{1 + \frac{\mu_{ijij}(\omega'_{ijd})}{\mu + \mu_T}} . \tag{42}$$

Note in Eqs. (39) and (40) that, at corresponding resonances, damped and undamped plate accelerations are evaluated at different frequencies. Consequently, to quantitatively interpret the reduction due to tile damping and water loading, the dependency of μ_{ijij} and r'_{ij} on frequency must be determined.

For the frequency range of Fig. 11, one may show that the plate wave number k_{ij} is always greater than the acoustic wave number k_o of the water. For k_{ij} greater than k_o, one may postulate from Eq. (18) that μ_{ijij} is approximately constant for $0 < \omega \leq \omega_{ij}$. Similarly, for k_{ij} greater than k_o, Eq. (17) reveals that $r_{ijk\ell}$ is directly proportional to frequency

squared for $0 < \omega \leq \omega_{ij}$.* Since r'_{ij} can be interpreted as a summation of many contributions of $r_{ijk\ell}$, it seems reasonable to assume that r'_{ij} is also proportional to frequency squared. Comparison of Eqs. (30) and (42) shows that the natural frequencies of the damped water-loaded plate are lower than those of the undamped plate as a result of the additional mass of the tile. Because of the dependence of r'_{ij} on frequency, one may conclude that the equivalent fluid damping $r'_{ij}(\omega'_{ijd})$ of the damped plate is less than the fluid damping $r'_{ij}(\omega'_{ij})$ of the undamped plate.

Clearly, then,

$$\frac{\mu + \mu_T + \mu_{ijij}(\omega'_{ijd})}{\mu + \mu_{ijij}(\omega'_{ij})} < \frac{\mu + \mu_T}{\mu} \tag{43}$$

and

$$\frac{r_d + r'_{ij}(\omega'_{ijd})}{r + r'_{ij}(\omega'_{ij})} < \frac{r_d}{r} \quad . \tag{44}$$

From Eqs. (39), (40), (43), and (44), it is apparent that the reduction of resonance amplitudes due to damping tiles is less in water than in air simply because the mass and damping added to the system by the tile are smaller proportions of the undamped system totals for water loading than for air loading.

The approximate theory developed above enables one to quantitatively separate the effects attributable to the properties of the damping tiles from those effects associated with water loading. Before utilizing the theory to analyze the experimental results, however, its applicability to the experimental conditions must be examined.

---

*This dependency of $r_{ijk\ell}$ on frequency is only valid for odd-odd plate modes. For even-odd or even-even plate modes, the dependency of r_{ijij} on frequency is not known. However, it can be shown from Eq. (17) that $r_{ijk\ell}$ is small and may be neglected for even-odd or even-even modes.

BOUNDARY CONDITIONS

The only difference between the theoretical model utilized to develop the approximate theory and the experimental model is in the boundary conditions at the edges of the plate. The theoretical model assumed a simply supported boundary condition and the experiment utilized a clamped-edge boundary. This difference effects a change in mode shapes, which in turn causes changes in α_{mn} and ω_{mn} that also affect μ_{mnqs} and r_{mnqs} (Eqs. (5), (6), (17), and (18)). However, because the general equation of motion (Eq. (1)) is applicable for any thin plate regardless of boundary conditions, one would expect to obtain a solution that, for either boundary condition, exhibits a similar dependence on the properties of the fluid and of the plate. It is concluded that the approximate theory may be applied to the measured acceleration spectra of the clamped-edge plate if the terms α_{mn} and ω_{mn} are redefined, and μ_{mnmn} and r'_{mn} are amended.

The fluid mass and damping of the vibration system are quantities to be computed from the measured acceleration spectra; consequently, for the clamped-edge plate, these terms can simply be denoted by μ'_{ijc} and r'_{ijc}, respectively, and substituted in Eqs. (30), (34), and (36). However, computation of μ'_{ijc} and r'_{ijc}, based on Eqs. (30), (34), and (36), requires knowledge of α_{mn} and ω_{mn}. Although ω_{mn} can be determined by inspection of the measured plate acceleration spectra, α_{mn} can not. Therefore the ratio of accelerations for air- and water-loaded plates must be utilized to compute the effects of water loading. Computations of this type cancel the dependence of acceleration spectra on the modal coefficients (α_{mn}) of the plate, but only the relative effects of water loading can be quantitatively evaluated.

To cancel the modal coefficients α_{mn}, however, one must show that the mode shapes of air- and water-loaded clamped-edge plates are similar. For a simply supported plate, the cross coupling between water and plate motion causes a difference in mode shapes for air- and water-loaded plates. Since the equivalent fluid damping r'_{mn} is a result of many contributions of r_{mnqs}, whereas the fluid mass μ_{mnmn} is not, one may hypothesize that the change in mode shapes results from the extensive cross coupling of the fluid resistive forces $r_{mnqs}\,\omega$. However, from the values of μ_{mnmn} and r'_{mn} listed in Tables 1 and 2, respectively, one may show that the fluid inertial forces $\mu_{mnmn}\,\omega^2$ are much greater than the fluid resistive forces $r'_{mn}\,\omega$. Because the autocoupled inertial forces dominate over the resistive forces, one may conclude that the difference in mode shapes for air- and water-loaded simply supported plates would be slight. To ensure that the difference in mode shapes

between air- and water-loaded clamped-edge plates is slight, it must be shown that the autocoupled fluid mass is the controlling mass term and that the fluid inertial forces are greater than the fluid resistive forces.

For high-frequency modal resonances, clamped-edge plate modes become similar in shape to simply supported plate modes. Thus, one may state that any difference between air- and water-loaded plate modes will be insignificant at high frequencies. However, at low-frequency modal resonances, where mode shapes of a simply supported plate are not similar to those for a clamped-edge plate, it must be assumed that any difference between air- and water-loaded clamped-edge plate modes will be small.

From the above and Eqs. (30), (34), (35), (36), and (37), the air- and water-loading ratios of natural plate frequencies, resonance amplitudes, and sharpness of resonances may be written, respectively, as

$$\frac{\omega_{mn}}{\omega'_{mn}} = \left[\frac{\mu + \mu_{mn}{}^{c}(\omega'_{mn})}{\mu}\right]^{1/2}, \tag{45}$$

$$\frac{\Phi_a(\omega_{mn})}{\Phi'_a(\omega'_{mn})} = \left[\frac{\mu + \mu'_{mn}{}^{c}(\omega'_{mn})}{\mu}\right]\left[\frac{r + r'_{mn}{}^{c}(\omega'_{mn})}{r}\right]^2, \tag{46}$$

and

$$\frac{Q(\omega_{mn})}{Q'(\omega'_{mn})} = \left[\frac{\mu}{\mu + \mu'_{mn}{}^{c}(\omega'_{mn})}\right]^{1/2}\left[\frac{r + r'_{mn}{}^{c}(\omega'_{mn})}{r}\right] \tag{47}$$

for a clamped-edge plate.

For the purpose of evaluating the effectiveness of tiles for damping a simply supported plate, the reduction in plate acceleration (accompanying an application of damping tiles) is expressed as a ratio of resonance amplitudes for the damped and undamped plates (Eqs. (39) and (40)). The ratio provides a measure of the damping-tile effectiveness that is independent of α_{mn}. Thus, Eqs. (39) and (40) may be written for a clamped-edge plate as

$$\Phi_a(\omega_{mn})/\Phi_{ad}(\omega_{mnd}) = \left[\frac{\mu + \mu_T}{\mu}\right]\left[\frac{r_d(\omega'_{mnd})}{r(\omega_{mn})}\right]^2 \quad (48)$$

and

$$\Phi'_a(\omega'_{mn})/\Phi'_{ad}(\omega'_{mnd}) = \left[\frac{\mu + \mu_T + \mu'_{mnc}(\omega'_{mnd})}{\mu + \mu'_{mnc}(\omega'_{mn})}\right]\left[\frac{r_d + r'_{mnc}(\omega'_{mnd})}{r + r'_{mnc}(\omega'_{mn})}\right]^2 . \quad (49)$$

In both Eqs. (48) and (49), r_d denotes damping of the tile-plate combination. For this analysis, r_d is assumed to be constant for air or water environments—that is, the water environment does not alter the damping properties of the tiles.

MASS AND DAMPING RATIOS

Table 3 lists both the ratio of the total mass of a water-loaded plate to that of an air-loaded plate and the ratio of the total damping of a water-loaded plate to that of an air-loaded plate. These ratios were computed for a few corresponding air- and water-loaded resonances from the undamped-plate acceleration spectra of Figs. 7, 8, 9, and 10 for both (x, y) measurement points. Computation of these ratios was based on Eqs. (45) and (46) in conjunction with the measured reduction in resonance frequencies and amplitudes accompanying water-loading. The ratios listed in Table 3 clearly indicate that the increases in both mass and damping due to water loading a plate are quite substantial. Further, the damping ratios for the first and third resonances are greater at the measurement point (x = 2.5 ft, y = 1.0 ft) than at the measurement point (x = 1.5 ft, y = 1.0 ft). Reference 7 shows that the damping of a point-excited, clamped-edge plate in air appears to decrease with increasing distance from the point of excitation. Inasmuch as the fluid damping r'_{mnc} is independent of its spatial location, the larger ratios of water- to air-loaded plate damping at (x = 2.25 ft, y = 1.0 ft) are a result of the decreased damping in air due to increased distance from the excitation point.

Table 4 lists, for both air- and water-loaded plates, the ratio of total mass of the damped plate to that of the undamped plate and the ratio of total damping of the damped plate to that of the undamped plate. These ratios were computed for the corresponding damped and undamped plate resonances in Figs. 7, 8, 9,

Table 3

RATIOS OF WATER-LOADED TO AIR-LOADED SYSTEM MASS AND OF WATER-LOADED TO AIR-LOADED SYSTEM DAMPING

x = 1.5 ft, y = 1.0 ft				x = 2.25 ft, y = 1.0 ft			
Resonance Frequencies (Hz)		$1+\frac{\mu'_{mn}c}{\mu}$	$1+\frac{r'_{mn}c}{r}$	Resonance Frequencies (Hz)		$1+\frac{\mu'_{mn}c}{\mu}$	$1+\frac{r'_{mn}c}{r}$
f_{mn}	f'_{mn}			f_{mn}	f'_{mn}		
110	48	5.25	6.16	107	48	4.98	11.9
--	--	--	--	175	69	6.45	2.64
255	119	4.58	1.20	245	117	4.40	1.55
320	230	1.93	3.04	--	--	--	--

and 10 for both points of measurement on the plate; the undamped air- and water-loaded plate resonances are identical with those listed in Table 3.

The masses of the plate and the damping tiles were measured to determine the mass ratio of damped to undamped plates in air. The damping ratio of damped to undamped plates in air was then computed by utilizing Eq. (48) in conjunction with the measured reduction in resonance amplitudes accompanying the application of damping tiles. To compute the ratios of mass and damping for damped and undamped water-loaded plates, one first computes the ratios of mass and damping for air- and water-loaded damped plates via the method utilized for the computations of Table 3. From these ratios and those listed in Table 3, where $(\mu + \mu_T)/\mu$ and r_d/r are known, one may easily compute the mass and damping ratios of damped to undamped plates in water. The increase, upon the application of damping tiles, in both total mass and total damping is less for water loading than the increase for air loading. (An exception is noted for the damping ratio of the third resonance.)

From the above and Table 3, the total mass and damping are effectively greater for a plate in water than for one in air; therefore any increase in the

Table 4

RATIOS OF DAMPED TO UNDAMPED TOTAL PLATE MASS AND OF DAMPED TO UNDAMPED TOTAL PLATE DAMPING FOR AIR- AND WATER-LOADED PLATES

(x = 1.5 ft, y = 1.0 ft)							
Resonance Frequencies (Hz)				$\frac{\mu + \mu_T}{\mu}$	$\frac{\mu + \mu_T + \mu'_{mnc}}{\mu + \mu'_{mnc}}$	$\frac{r_d}{r}$	$\frac{r_d + r'_{mnc}}{r + r'_{mnc}}$
f_{mn}	f_{mnd}	f'_{mn}	f'_{mnd}				
110	92	48	47	1.43	1.05	1.98	1.23
--	--	--	--	--	--	--	--
255	210	119	118	1.43	0.98	1.33	1.47
320	310	230	230	1.43	1.35	2.05	1.19
(x = 2.25 ft, y = 1.0 ft)							
Resonance Frequencies (Hz)				$\frac{\mu + \mu_T}{\mu}$	$\frac{\mu + \mu_T + \mu'_{mnc}}{\mu + \mu'_{mnc}}$	$\frac{r_d}{r}$	$\frac{r_d + r'_{mnc}}{r + r'_{mnc}}$
f_{mn}	f_{mnd}	f'_{mn}	f'_{mnd}				
107	90	48	47	1.43	1.05	2.65	1.30
175	138	69	66	1.43	0.97	2.97	2.31
245	207	117	114	1.43	1.07	2.05	2.50
--	--	--	--	--	--	--	--

total mass and damping of the vibration system due to damping tiles is proportionally less for water loading than for air loading. Inasmuch as an increase in damping and mass causes a lowering of peak spectral levels at resonance, the smaller reduction of peak levels for water loading is attributable to the tiles' proportionally less effective contribution to the system's mass and damping. However, a comparison of Figs. 8 and 10 will show that there is a greater degree of resonance amplitude reduction (accompanying the application of damping tiles) for a plate in water than for one in air at frequencies greater than 1500 Hz; the theory does not account for this discrepancy and the reason for it was not determined.

From the ratios of mass and damping listed in Table 4, one may show that the reduction (accompanying the application of damping tiles) in mean-squared acceleration within the bandwidth of a particular resonance is less for water loading than for air loading. Here, the mean-squared acceleration $\langle \alpha^2_{mn} \rangle$ within the bandwidth of a particular resonance is proportional to the height of resonance Φ_{amn} multiplied by its half-power-point bandwidth. Thus, from Eqs. (45), (46), and (47) one may show, for water loading, that

$$\frac{\langle a'^2_{mn} \rangle}{\langle a'^2_{mnd} \rangle} = \left[\frac{\mu + \mu_T + \mu'_{mnc}(\omega'_{mnd})}{\mu + \mu'_{mnc}(\omega'_{mn})} \right]^2 \left[\frac{r_d + r'_{mnc}(\omega'_{mnd})}{r + r'_{mnc}(\omega_{mn})} \right] \tag{50}$$

and, for air loading, that

$$\frac{\langle a^2_{mn} \rangle}{\langle a^2_{mnd} \rangle} = \left[\frac{\mu + \mu_T}{\mu} \right]^2 \left[\frac{r_d(\omega_{mnd})}{r(\omega_{mn})} \right] . \tag{51}$$

Then, from the damping and mass ratios shown in Table 4, one may show by Eqs. (50) and (51) that

$$\frac{\langle a'^2_{mn} \rangle}{\langle a'^2_{mnd} \rangle} < \frac{\langle a^2_{mn} \rangle}{\langle a^2_{mnd} \rangle} . \tag{52}$$

Consequently, both the fluid mass and damping limit not only damping-tile reductions in resonance amplitudes but, also, mean-squared acceleration within the bandwidth of a resonance.

SUMMARY AND CONCLUSIONS

Comparison of the measured damped and undamped plate-acceleration spectra for both air and water environments revealed that the reduction in resonance amplitudes resulting from the application of damping tiles to a plate was less for water loading than for air loading. Because plate vibration levels are directly related to vibration-induced pressure levels in the fluid surrounding a plate, the amount of reduction in acceleration levels provides a measure of damping-tile effectiveness. Consequently, a decrease in the reduction of resonance amplitudes for water loading was interpreted as a decrease in the effectiveness of damping tiles.

The theoretical model was utilized to explain the decreased effectiveness of damping tiles observed for water loading. Based on the theoretical model, computed acceleration spectra were compared for air- and water-loaded undamped plates to determine the effects of water loading. An approximate theory was developed from the theoretical model, in conjunction with computed spectra, to quantitatively evaluate both the effects of water loading and the effects of applying damping tiles to a water-loaded plate.

From the theoretical model, it was determined that the pressure field induced by plate vibrations produces additional forces on the plate; these forces were interpreted as additional mass and damping of the plate. Applying damping tiles to a plate was also interpreted as an increase to the mass and damping of the plate. By using the approximate theory as a basis, the additional fluid mass was found to be equal to or up to five times greater than the mass of the plate, and the additional fluid damping was found to be equal to or up to ten times greater than the damping of the plate. Clearly, water loading substantially increases the mass and damping of the plate.

The approximate theory shows that an increase in mass alone affects the plate acceleration at resonance by

- lowering resonance amplitudes,
- increasing the sharpness of resonance, and
- lowering resonance frequencies.

Additionally, an increase in damping alone causes

- a lowering of resonance amplitudes and
- a decrease in the sharpness of resonance.

The approximate theory also shows that the combined effect of increasing both the mass and damping of a plate is to decrease the mean-squared acceleration associated with the half-power bandwidth of a resonance. These effects were in agreement with the measured spectra.

Total mass and damping are effectively greater for a plate in water than in air; therefore the increase in total mass and damping to a plate due to the application of damping tiles is proportionately less for water loading than for air loading. Inasmuch as an increase in the mass and damping of the plate causes a lowering of both resonance amplitudes and mean-squared acceleration associated with the half-power bandwidth of resonances, the fluid mass and damping are responsible for the decreased effectiveness of damping tiles in water.

In most practical applications of damping tiles, the mass and damping associated with a water environment are large compared with the mass and damping of plating. Consequently, it is apparent that, in determining the effectiveness of damping tiles applied to plating in water, measurements of the properties of damped and undamped plates in air alone are insufficient. The approximate theory enables one to quantitatively evaluate the fluid mass and damping based on measurements of resonance vibration amplitudes. Reference 7 describes a technique of measuring the sharpness of resonance Q for air- and water-loaded clamped-edge plates. This measurement, in conjunction with the approximate theory defining the Q of air- and water-loaded plates, can also be used to qualitatively evaluate the fluid mass and damping. Either of these combined experimental and theoretical methods for determining the effects of water loading on plate vibrations should be more accurate than any purely theoretical assessment of the effects of water loading. Further, it can be shown that the approximate theory may be applied to most thin plates regardless of the boundary conditions. The only limitation imposed on the theory is that the wave number of the plate must be greater than the acoustic wave number of the fluid environment; in most practical applications, however, the limit imposed on the wave number of the plate is not approached. Consequently, the theory can be a valuable tool for determining the effects of water loading with respect to assessing the effectiveness of damping tiles for reducing vibration of plates in water.

REFERENCES

1. G. Maidanik, "Response of Ribbed Panels to Reverberant Acoustic Fields," Journal of the Acoustical Society of America, vol. 34, no. 6, June 1962, p. 818.

2. P. H. White, Cross-Spectral Density of Pressure Field Behind an Infinite Plate Excited by Boundary Layer Turbulence, Measurement Analysis Corporation Report No. 602-01, Los Angeles, 26 September 1966.

3. H. G. Davies, Acoustic Radiation from Fluid-Loaded Rectangular Plates, Acoustics and Vibration Laboratory Report No. 71476-1, Massachusetts Institute of Technology, Cambridge, Mass., December 1969.

4. Damping and Flexural Vibrations in Plates by Free and Constrained Visco-Elastic Layers, Final Report on Phases I-III, Bolt, Beranek and Newman Report No. 632, Los Angeles, 28 May 1959.

5. F. Irgens and R. S. Brand, Coupling of Acoustic Fields and Vibrating Membranes and Plates, School of Engineering Report, University of Connecticut, Storrs, Conn., 1 July 1968.

6. W. A. Strawderman, "Turbulence-Induced Plate Vibrations: An Evaluation of Finite and Infinite-Plate Models," Journal of the Acoustical Society of America, vol. 46, no. 5, November 1969, pp. 1294-1307.

7. R. Steinbeck, "Techniques for Measuring Damping of Finite Plates in Air and Water," NUSC Technical Memorandum No. TD12-290-71, 1 September 1971.

REVERSE BLANK